Journal of Applied Electrochemistry **30**: 101–105, 2000.
© 2000 *Kluwer Academic Publishers. Printed in the Netherlands.*

Bipolar plate materials for solid polymer fuel cells

D.P. DAVIES, P.L. ADCOCK, M. TURPIN and S.J. ROWEN
Fuel Cell Research Group, Department of AAETS, Loughborough University, Loughborough, Leicestershire, LE11 3TU, Great Britain

Received 14 March 1999; accepted in revised form 18 July 1999

Key words: bipolar plate, passive film, solid polymer fuel cell, stainless steel

Abstract

The interfacial ohmic losses between the bipolar plate and the MEA can significantly reduce the overall power output from a SPFC. For graphitic bipolar plate materials, these losses are insignificant relative to stainless steel, where the existence of a passive film on the surface greatly reduces electrical conductivity. In this paper we have evaluated different bipolar plate materials, and present long-term fuel cell data for Poco® graphite, titanium, 316 and 310 stainless steel. The properties of the passive film on the surface of 316 and 310 stainless steel are markedly different. Although both were adequately corrosion resistant in a fuel cell environment, 310 tended to produce higher fuel cell performance and like 316, no degradation was observed after 1400 h testing. Analysis of the passive film indicated that this increased performance was related to the decreased thickness of the oxide film.

1. Introduction

The solid polymer fuel cell (SPFC) is regarded as a possible future high efficient, low pollution power source, for stationary and transportation applications. The operating principles of a SPFC are straightforward. It involves the generation of electricity via the electrochemical reaction between a fuel gas (normally hydrogen) and oxygen. Their importance is illustrated by the intense interest shown by the major car manufacturers, who are now adopting fuel cells as the best route to combat pollution [1]. However, to be cost-competitive for all applications, there is a need for cheaper materials and lower fabrication costs. Prismatic bipolar stack design is considered to be the most volume efficient form that a SPFC can take, offering the benefits of modularity and relatively simple construction method. A key component of this is the bipolar plate, but with technology based on machined graphitic flow field plates accounting for as much as 60% of the stack costs, this is one area where cost is required to be significantly reduced [2].

A bipolar plate is a multifunctional component of a SPFC. The raised area of the bipolar plate contacts the macrodiffusion part of the membrane electrode assembly (MEA), with channels providing gas access to the gas diffusion electrode (GDE), while also removing excess water produced by the electrochemical reaction between hydrogen and oxygen. Consequently, an ideal bipolar plate would exhibit excellent corrosion resistance, thermal compatibility with other cell components and provide electrical contact with the macrodiffuser with minimum electrical resistive loss [3]. Current plate designs are generally based on either metallic (principally stainless steel) or graphitic materials. Properties of these materials affect the electrochemical response of a SPFC. Graphite is good in electronic conductivity, corrosion resistance and also low weight, but lacks mechanical strength. Conversely, stainless steel plates have relatively high strength, but due to their ability to self passivate on exposure to air and the anodic potential imposed on the plate during fuel cell operation, an insulating passive film that may increase in thickness over time, forms on the plate. This reduces electronic conductivity and consequently lowers SPFC efficiently [4]. Also, there is concern that the use of metallic plates may introduce problems associated with corrosion.

The main fuel cell developers are pursuing this two material pathway although it is not yet clear which approach will be favoured in the long-term. With cost targets for transport applications quoted at \$50 kW^{-1} and performance criteria of 1 kW dm^{-3} and 1 kW kg^{-1}, an ideal plate would incorporate the merits of metal and graphite [5, 6]. A stainless steel approach is currently being adopted by ourselves and others [7–10]. Hence, in this paper we detail our research findings on a number of commercially available stainless steel alloys, suggested as possible candidate materials for use in SPFCs, and present long-term performance data for the most promising.

2. Experimental details

2.1. *Electrical contact resistance of bipolar plate materials*

A method for quick evaluation of electrical interfacial resistance between each candidate material and the gas diffusion media (Carbel® CL), which roughly simulated a typical SPFC arrangement, was developed. Two pieces of Carbel® CL were sandwiched between the two test samples (Figure 1). These were thoroughly cleaned using isopropyl alcohol, followed by multiple washes with distilled water and dried in air overnight. An electrical current (5 A) was passed through this arrangement and by measuring the potential difference across the plate samples, while the compaction force was gradually increased, it was possible to calculate the interfacial resistance dependency on compaction force according to the following equation:

$$R = \frac{VA_s}{I} \tag{1}$$

where R is the electrical contact resistance, V the potential across the metal samples, I the current and A_s the surface area. The compaction force was applied using a Lloyd Instruments LRX 5K tensometer.

This method was only used as a comparative guide to interfacial resistance and, as such, no strict resistive data should be quoted. As can be seen from Figure 1, the total measured resistive losses are the sum of three interfacial components (two between the samples and Carbel® CL, and one between Carbel® CL and Carbel® CL).

2.2. *MEA pretreatment*

Gore Primea® 5510 membrane electrode assemblies with Carbel® CL gas diffusion media was selected as a standard MEA for the long-term compatibility testing. Prior to electrochemical performance evaluation, it was essential to hydrate the membrane to enable proton conduction. Thus, for each new assembly, the dry MEA was preconditioned to ensure the optimum hydration state, according to the following. On start up at ambient hydrogen and air pressure, the temperature of the cell and humidification chambers were gradually raised to 60 °C; ensuring that the temperature differential was within 5 °C to avoid cell drying/flooding. At this temperature, the cell potential was cycled between 0.6 V and 0.3 V while monitoring performance with respect to time; changing potential when a steady state power output was achieved. A steady cell performance was achieved after several 0.3/0.6 V conditioning steps. After leaving overnight, the pressure and temperature of each cell were maintained at the test operating conditions, and subjected to a fixed current density, unless otherwise stated.

2.3. *Fuel cell testing*

A purpose built multiarray endurance rig, with the capability for simultaneous long-term testing of upto eight identical independent cells, was used to determine actual fuel cell data for the various bipolar plate materials. For each material, a pair of fuel cell plates was prepared with a machined gas track design, and thoroughly cleaned using an organic solvent prior to use. On assembly, a fixed compaction force (220 N cm^{-2}) was imparted on each MEA, the purpose of which was two fold. First, to provide adequate sealing of the pressurised cell and secondly to reduce ohmic losses incurred by poor contact between the MEA and the bipolar plate. Following preconditioning of the MEA, the long-term test conditions were set as summarized in Table 1. All cells (active surface area 11.8 cm^2) were galvanostatically controlled with fixed interval monitoring of cell potential recorded via PC based data acquisition software. The test procedure was a cycle of five days where each cell was tested at a constant current density of 0.7 A cm^{-2}, followed by a period of two days where the rig was shut down (0 A and no reactant flow).

Full polarization data was taken periodically throughout the long-term testing. The first set was recorded immediately after the preconditioning step, and periodically at points thereafter (typically every 100 h). The limitations of the flow controllers meant that it was almost impossible to maintain the stated stoichiometric flow of reactants throughout the current density range. Thus, a fixed flow was maintained for all current

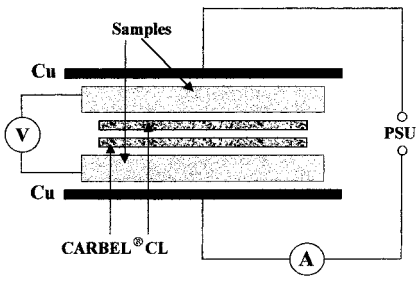

Fig. 1. Schematic of test assembly for comparing electrical surface resistance of each material.

Table 1. Endurance rig operating conditions

MEA	Gore Primea® Series 5510 (based on Gore-Select® membranes), 0.3 mg cm^{-2} Pt. Carbel® CL as gas diffusion media
Hydrogen pressure	3 bar (g)
Air pressure	3 bar (g)
Hydrogen flow	0.08 SLPM (stoichiometry 1.5)
Air flow	0.42 SLPM (stoichiometry 3)
Cell temperature	50 °C
Humidification	100% RH for H_2 and Air
Compaction 'force'	220 N cm^{-2}
Current density	0.7 A cm^{-2}

loadings. For hydrogen this was 0.08 SLPM and air 0.8 SLPM.

3. Results and discussion

3.1. *Interfacial resistance losses*

Figures 2 and 3 show the relationship between compaction force and interfacial resistance between the Carbel® CL and the tested samples. Materials with the lowest and highest interfacial resistance are detailed in Figure 2 and Figure 3, respectively. The stainless steel samples all displayed increased resistance relative to Poco® graphite, due to the existence of the passive film. However, depending on the elemental composition of the sample, there was a large variation in electrical resistance. By consideration of the values at 220 N cm^{-2} (the compaction 'force' imposed for the fuel cell experiments), the relative interfacial resistance decreased in the order 321 > 304 > 347 > 316 > Ti > 310 > 904 > Incoloy 800 > Inconel 601 > Poco® graphite.

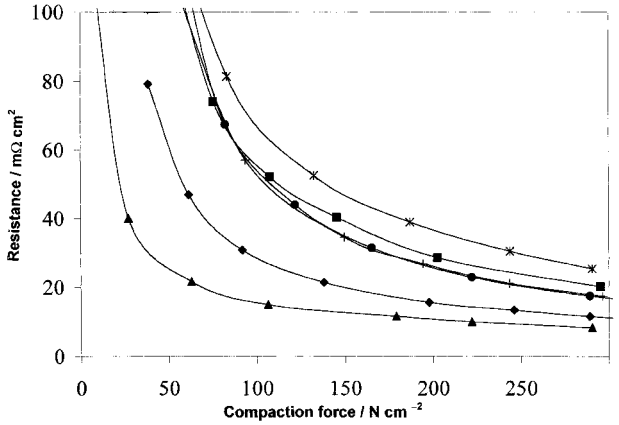

Fig. 2. Interfacial resistance dependency on compaction force: materials with lowest interfacial resistance. Key: (◆) Inconel 601; (▲) Poco; (+) 904; (●) Incoloy 800; (■) 310; (×) titanium.

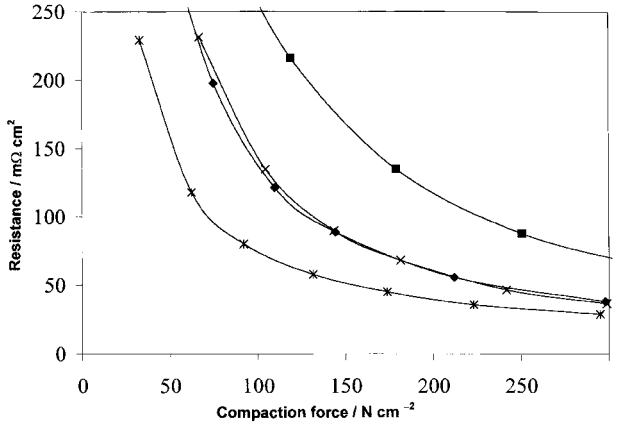

Fig. 3. Interfacial resistance dependency on compaction force: materials with highest interfacial resistance. Key: (◆) 347 SS; (×) 304 SS; (■) 321 SS; (×) 316 SS.

The variation in the interfacial resistance throughout the range of stainless steel sample was most likely due to the composition of the alloy, in particular in the region of the passive film. Despite confusion in the literature as to the exact nature of this film, it is generally regarded that passivation results from the formation of an insoluble oxide film on the surface. For stainless steel the principle components of this film are iron, nickel and chromium oxides [11–15]. It was suspected that the cumulative properties of these oxides were inhibiting the electrical conductivity. Thus, surface analysis of the stainless steel samples by Auger electron spectroscopy (AES) was used to provide details of variations within the oxide film. By use of an AES depth profiling technique, differences in the elemental composition of the oxide film could be deduced. Further stainless steel samples were prepared (1 cm^2) and pretreated in identical fashion to that for the bipolar plate. If the physical properties of the oxide film affected the surface resistivity, AES depth profiling would give information as to the relative thickness of the passive film. Data shown in Figure 4 details the normalized oxygen concentration, at the given depth within the film, given by this technique.

Although it was difficult to deduce the exact thickness of the oxide film solely from AES, it was evident that the concentration of oxygen varied significantly. With AES, data is given for the normalized atomic percentage of the constituents at a given depth. For the high alloy materials, the oxygen was not as prominent as that illustrated for the other grades of stainless steel, which suggests that the passive film was thinner in these samples. From these results we can summarize that the passive film decreased in thickness according to the order 321 > 304 > 316 > 347 > 310 > 904 > Incoloy 800 > Inconel 601. This general trend translates to the measured interfacial resistance losses discussed earlier.

3.2. *Electrochemical performance of materials*

Immediately following the interfacial resistance analysis, bipolar plate samples were assembled in the long-term

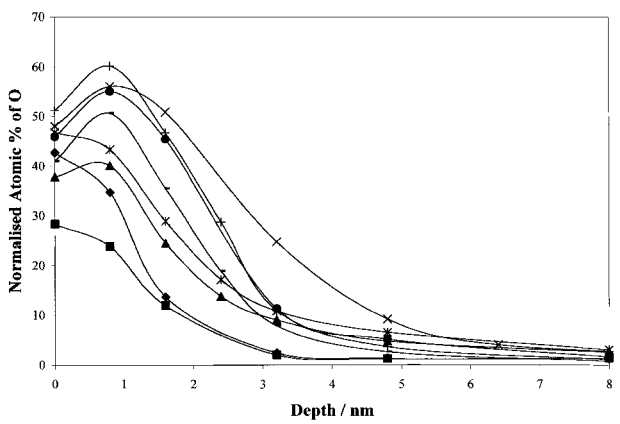

Fig. 4. Depth profile for oxygen with passive films. Key: (◆) Incoloy 800; (▲) 904; (×) 310; (+) 321; (■) Incoloy 601; (×) 304; (●) 316; (■) 347.

endurance rig. The four materials chosen for this initial evaluation were Poco® graphite, titanium, 316 and 310 stainless steel. Despite exhibiting reduced interfacial resistance, the high alloyed samples (Inconel 601 and Incoloy 800) were considered relatively too expensive to pursue at this stage, but would be evaluated at a later date. Each fuel cell arrangement was duplicated to verify consistency of results, which in all cases was within experimental error (5%). 316 stainless steel and Poco® graphite were selected as most results presented in the literature use these materials. 310 stainless steel (25% Cr, 20% Ni), a cost competitive alternative to the traditionally used 316 stainless steel, illustrated lower interfacial resistance losses as well as greater resistance to corrosion and oxidation. Titanium has the advantage of being significantly lighter in weight than stainless steel yet retains mechanical strength, thus would be particularly advantageous for automotive applications. Figure 5 shows the initial polarization response for these materials, generated once the membranes had been pretreated.

The polarization data taken before long-term evaluation corroborates that the difference in fuel cell performance was due to the surface properties of the bipolar plate material. Poco® graphite, with the lowest surface resistive losses, produced the highest potentials, with increased polarisation observed for the metal plates in the order Poco® graphite < 310 < Ti < 316. This followed the trend seen with the measured surface resistance. Of most interest from this study was the significant difference between 310 and 316 stainless steel. At a current density of 0.7 A cm^{-2}, the cell containing 316 stainless steel bipolar plates had a potential of 485 mV, whilst 310 stainless steel was at 606 mV. This increased performance for 310 stainless steel was maintained throughout the long-term testing (Figure 6), where although neither samples showed any performance degradation (over 1200 h), higher potentials were consistently achieved with 310 stainless steel. If the stainless steel was corroding or passivating further over time, the surface resistance would increase, and consequently the cell potential would decrease.

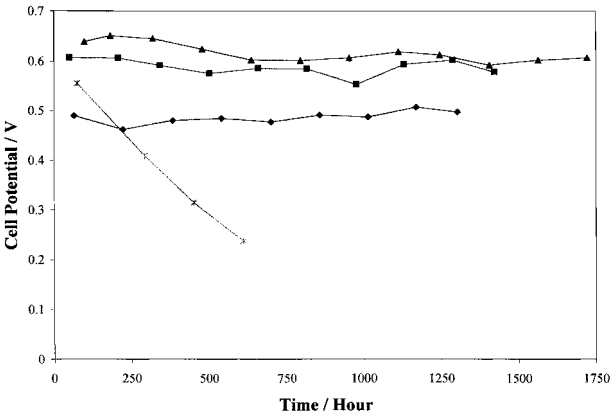

Fig. 6. Average cell potential for periods where cells were under load. Key: (▲) Poco® graphite; (■) 310 SS; (◆) 316 SS; (×) titanium.

Figure 5, gives the average cell potential taken for each five day period where cells were under load (0.7 A cm^{-2}). This illustrates that there was very little change in performance for Poco® graphite, 316 and 310 stainless steel. Thus, despite concerns regarding corrosion and how this could inhibit performance, 316 and 310 stainless steel have been shown to provide adequate protection in a fuel cell environment. Post fuel cell analysis of the membrane also indicated no stainless steel corrosion products had leached into the membrane.

Full polarization data recorded at sometime into the long-term test, shows that there was very little change from initial data in terms of the current/potential relationship for the stainless steel samples (Figure 7). After 1300 h, the 316 stainless steel cell had a potential of 487 mV, while for 310 stainless steel, the potential was 597 mV at 0.7 A cm^{-2}. This was also the case for Poco® graphite, but with titanium, a much-decreased performance was observed.

After running each arrangement for the specified period, the cells were dismantled and the interfacial resistance for each material was measured (Figure 8). These measurements supported our findings from the

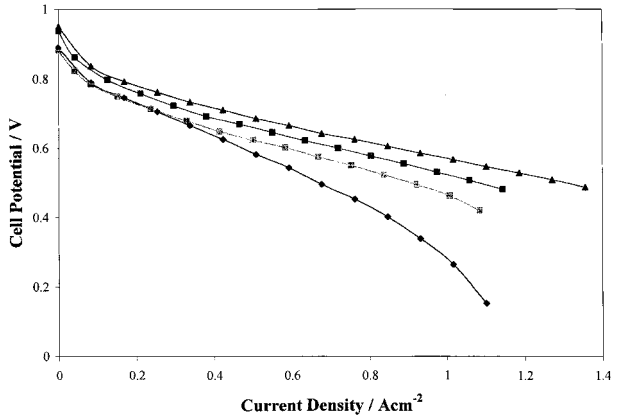

Fig. 5. Polarization plot for each cell arrangement before long-term testing. Key: (▲) Poco® graphite; (◆) 316 SS; (■) 310 SS; (×) titanium.

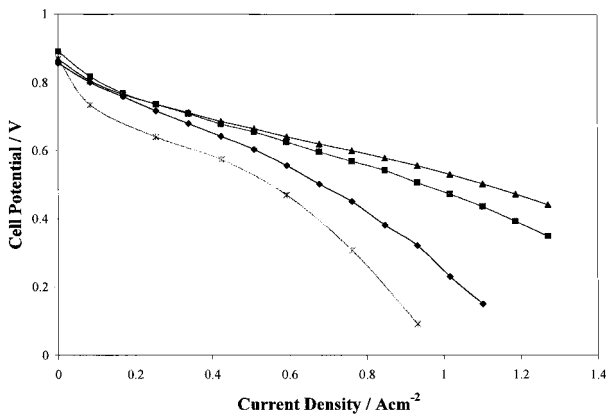

Fig. 7. Polarization plot for each cell arrangement after long-term testing. Key: (▲) Poco® graphite; (◆) 316 SS, 1300 h; (■) 316 SS, 1300 h; (×) titanium, 400 h.

Table 2. Data for bipolar plate materials*

Name	% Composition†			Interfacial resistivity/mΩ cm^2		Voltage at 0.7 A cm^{-2}/V	
	Cr	*Ni*	*Other*	*Before*	*After*	*Before*	*After*
304	18–20	8–10.5		51	–		
310	24–26	19–22		26	28	0.606	0.597
316	16–18	10–14	Mo	37	44	0.485	0.487
321	17–19	9–12	Ti	100	–		
347	17–19	9–12	Nb	53	–		
904L	19–23	23–28	Mo	24	–		
Incoloy 800	19–23	30–35	Al, Cu, Ti	23	–		
Inconel 601	21–25	58–63	Al, Cu	15	–		
Titanium				32	250	0.565	0.381
Poco® graphite				10	10	0.639	0.620

* Stainless steel grades using the American Iron and Steel Institute (AISI) convention. Surface resistance measured at 220 N cm^{-2} using the technique described

† Balance iron [16]

fuel cell experiments. For Poco® graphite, 316 and 310 stainless steel, there was little change in surface resistance, but for titanium a significant increase was measured. This was attributed to the growth of the electrically insulating oxide film. Table 2 summarizes the link between these changes in interfacial resistance and electrochemical fuel cell performance, with the chemical composition of the bipolar plate.

4. Conclusions

We have shown how the properties of the bipolar plate material effect the power capability of a SPFC. In particular, we have shown that 316 and 310 stainless steel can be used as a bipolar plate materials in a SPFC without any detectable long-term performance loss due to corrosion. Most importantly, the higher potentials associated with 310 stainless steel suggests a significant improvement over 316 stainless steel in terms of fuel cell power output. This was due to a thinner passive film on the 310 alloy. Thus, it is feasible to suggest that the use of 310 stainless steel would improve the performance of low cost metallic bipolar plate SPFCs, with a high power/volume ratio (>1 kW dm^{-3}), and with satisfactory corrosion resistance.

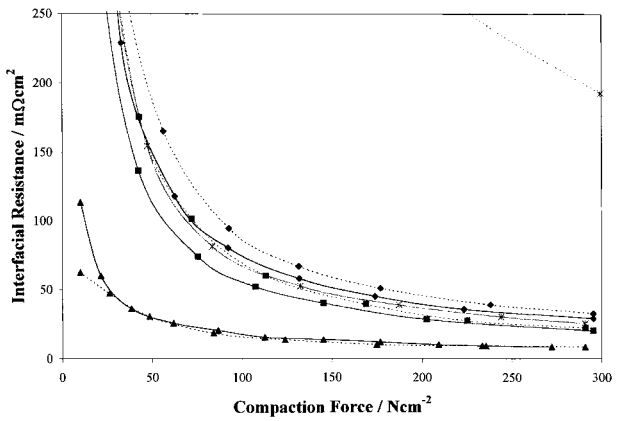

Fig. 8. Interfacial resistance variation due to running in SPFC. Key: (◆) 316 SS at $t = 0$; (■) 310 SS at $t = 0$; (×) titanium at $t = 0$; (▲) Poco® graphite at $t = 0$ (◆) 316 at $t = 1400$ h; (■) 310 at $t = 1400$ h; (×) titanium at $t = 600$ h (▲) Poco® graphite at $t = 1600$ h.

Acknowledgements

The financial support provided by the Engineering and Physical Sciences Research Council (EPSRC) is greatly appreciated. The authors wish to thank the Institute of Surface Science and Technology (ISST) at Loughborough University for conducting the Auger Electron Spectroscopy experiments. Gore-Select, Primea and Carbel are trademarks of W.L. Gore and Associates, Inc.

References

1. T.R. Ralph and G.A. Hards, *Chem. Indust.* (May 1968), 334.
2. B. Bahar, Abstracts, 'Commercialising Fuel Cell Vehicles' (Chicago Sept. 1996).
3. A.J. Appleby and F.R. Foulkes, 'Fuel Cell Handbook' (Krieger, 1993).
4. M.G.S. Fereira and C.A. Melendres, 'Electrochemical and Optical Techniques for the Study and Monitoring of Metallic Corrosion' (Kluwer Academic, Dordrecht, 1991), p. 289.
5. C.E. Borrini-Bird, *J. Power Sources* **61** (1996) 33.
6. K. Prater, *J. Power Sources* **51** (1994) 129.
7. R.K.A.M. Mallant, F.G.H. Koene, C.W.G. Verhoeve and A. Ruiter, Extended Abstracts, Fuel Cell Seminar, San Diego, CA (1994), p. 503.
8. C. Zawodzinski, M.S. Wilson and S. Gottesfeld, Extended Abstracts, Fuel Cell Seminar, Orlando, FA (1996).
9. K. Prater, *J. Power Sources* **61** (1996) 105.
10. R. Hornung and G. Kappelt, *J. Power Sources* **72** (1998) 20.
11. N. Ramasubramanium, N. Preocanin and R.D. Davidson, *J. Electrochem. Soc.* **132** (1985) 793.
12. I. Olefjord and L. Wegrelius, *Corros. Sci.* **31** (1990) 89.
13. A.M.P. Simões, M.G.S. Ferraria, G. Lorang and Da Cunha Belo, *Electrochim. Acta* **36** (1991) 315.
14. G. Lorang, Da Cunha Belo, A.M.P. Simões and M.G.S. Ferraria, *J. Electrochem. Soc.* **141** (1994) 3347.
15. M.G.S. Ferraria,. T. Moura e Silva, A. Catarina, M. Pankuch and C.A. Melendres, *J. Electrochem. Soc.* **139** (1992) 3146.
16. Source Book on Stainless Steel, American Society for Metals, (1976).